

Continuous rainbow RABBITT investigation of resonant states in He and H₂

Vladislav V. Serov¹ and Anatoli S. Kheifets²

¹*Department of Medical Physics, Saratov State University, Saratov 410012, Russia** and

²*Research School of Physics, The Australian National University, Canberra ACT 2601, Australia[†]*

(Dated: February 14, 2025)

We employ Reconstruction of Attosecond Beating By Interference of Two-photon Transitions with an advanced energy resolution (rainbow RABBITT) to resolve under-threshold discrete excitations and above-threshold autoionizing states in the He atom and the H₂ molecule. Both below and above the threshold, the whole series of resonances is reconstructed continuously and at once by the parity based separation of the two-photon ionization amplitude. This allows for an efficient extraction of the RABBITT magnitude and phase parameters without the need for adjusting the laser photon frequency. The latter parameters are then used to test the validity of the logarithmic Hilbert transform which relates the RABBITT phase and magnitude in the resonant region.

PACS numbers: 32.80.Rm 32.80.Fb 42.50.Hz

I. INTRODUCTION

Reconstruction of Attosecond Beating by Interference of Two-photon Transitions (RABBITT) is a well established two-photon interferometric technique. In this technique, like in the pioneering work [1], an atomic target is ionized with a comb of odd XUV harmonics $(2q \pm 1)\omega$ from an attosecond pulse train (APT) and probed with a dressing IR laser field with the carrier frequency ω . The primary ionization results in regularly spaced harmonic peaks in the photoelectron energy spectrum. The dressing field adds sidebands (SBs) centered at $2q\omega$. The height of the sidebands oscillates with XUV/IR delay τ at twice the IR photon frequency

$$S_{2q}(\tau) = A + B \cos[2\omega\tau + C] \quad , \quad C = 2\omega\tau_a \quad . \quad (1)$$

Here $A, B > 0$ are the RABBITT magnitudes parameters and C is its phase which is related with the atomic time delay τ_a .

The conventional RABBITT analyzes the whole SB as a single entity and determines the parameters in Eq. (1) as a function of the SB order $2q$. The rainbow RABBITT, or r RABBITT, goes one step further. It looks inside the SB and determines the parameters in Eq. (1) as functions of the photoelectron energy across the given SB. Experimentally, such a detailed energy-resolved analysis of SB's is achieved by an enhanced spectral resolution which can bring a wealth of additional information. In particular, it can help to disentangle various ionization pathways involving autoionizing resonances [2–5], below threshold discrete states [6] and fine-structure splittings [7, 8] The same technique can be beneficial when the presence of multiple ionization channels leads to spectral congestion in atoms [9] and molecules [10]. Similarly to r RABBITT, an advanced spectral resolution of SB's can

be achieved in conventional RABBITT by fine tuning of the laser photon frequency [11–13].

Simultaneous energy resolution of several SB's in r RABBITT is not possible at present neither experimentally nor theoretically. Each SB should be resolved individually by adjusting the laser carrier frequency ω appropriately. In the present theoretical work, we lift this restriction and overcome such an obstacle. We demonstrate that all the SB's in the photoelectron spectrum can be resolved simultaneously and at once.

Our simulations are based on a numerical solution of the time-dependent Schrödinger equation (TDSE) driven by a combination of the ionizing XUV and dressing IR laser fields. The ionizing field is generated by an APT composed of a number of short XUV pulses. A weak dressing field is represented by a femtosecond IR pulse. By performing several TDSE calculations at varying ω at sufficiently broad, but not yet overlapping primary and secondary peaks, it becomes possible to obtain the RABBITT parameters continuously across the photoelectron spectrum of interest. It is this strategy that is commonly employed in r RABBITT experiments e.g. in [4, 6].

Meanwhile, unlike in the experiment, the TDSE simulations give us access to the ionization amplitudes. The primary harmonic peaks in the photoelectron spectrum arise from the constructive interference of the one-photon ionization amplitudes which interfere destructively in the gaps between these peaks. These gaps are filled by the SB's which therefore originate solely from the two-photon ionization amplitudes. The latter amplitudes can be obtained by subtracting the single-photon XUV-only ionization amplitude from the combined XUV+IR amplitude. Such a subtraction is not possible experimentally as the two-photon ionization cross-section would contain an XUV/IR interference term. For the amplitude subtraction, it is suffice to use a sufficiently short XUV pulse with a broad spectrum [19, 20]. The probability of the two-photon ionization process will be the function of the phase shift between the XUV and IR pulses just as prescribed by Eq. (1). In this way, it is possible to obtain the RABBITT parameters continuously across the whole

*Electronic address: vladislav.serov@gmail.com

[†]Electronic address: A.Kheifets@anu.edu.au

photoelectron spectrum. We refer to such an approach as a continuous *r*RABBITT or *cr*RABBITT.

In the case of an atom or a symmetric molecule, instead of subtraction, the two-photon process amplitude can be isolated based on its parity. If the parity of the initial state is positive, the parity of the one-photon absorption amplitude will be negative, while the two-photon process amplitude will have positive parity. This approach requires even fewer calculations.

We demonstrate the advantages of the *cr*RABBITT technique by studying formation of autoionizing states (AIS) in the He atom and the H₂ molecule. In addition, we look under the threshold and map a series of discrete one-electron excitations. Such under-threshold or *u*RABBITT investigations showed their great potential in mapping the target atom electronic structure [6, 11, 14–18]

After the *cr*RABBITT phase and amplitude parameters are obtained across the whole photoelectron spectrum, they can be used to test the validity of the Kramers-Kronig relation in the form of the logarithmic Hilbert transform (LHT). This relation connects the photoionization phase and amplitude in the resonant region [21, 22]. So far this relation has been tested for single-photon ionization. The present work demonstrates the first successful application of the LHT to two-photon resonant ionization processes.

The rest of the paper is organized as follows. In Sec. II we describe our computational technique. Our numerical results are presented in Sec. III. The latter section is divided into Sec. III A and Sec. III B dealing with autoionizing states and below-threshold excitations, respectively. We conclude in Sec. IV by summarizing our main findings and outlining possible extension of the present work.

II. COMPUTATIONAL TECHNIQUE

As in our previous applications [23, 24], we solve numerically the two-electron TDSE

$$i(\partial/\partial t)\Psi(\mathbf{r}_1, \mathbf{r}_2, t) = \hat{H}\Psi(\mathbf{r}_1, \mathbf{r}_2, t), \quad (2)$$

where the Hamiltonian \hat{H} contains the single-electron ionic parts $\hat{h}_0(\mathbf{r})$, the electron-electron interaction $v(\mathbf{r}_1, \mathbf{r}_2)$ and the interaction with an external field $\hat{w}(\mathbf{r}, t) = -\mathbf{E}(t) \cdot \mathbf{r}$ expressed in the coordinate gauge.

Solution of the TDSE (2) is sought as a multi-configuration expansion

$$\Psi(\mathbf{r}_1, \mathbf{r}_2, t) = \sum_{n=1}^{N_s} [\psi_n(\mathbf{r}_1, t)\phi_n(\mathbf{r}_2) + (-1)^S \phi_n(\mathbf{r}_1)\psi_n(\mathbf{r}_2, t)], \quad (3)$$

built from the ionic eigenstates satisfying the stationary Schrödinger equation $\hat{h}_0\phi_n(\mathbf{r}) = \epsilon_n\phi_n(\mathbf{r})$. Further details on construction of the multiconfiguration basis and its symmetrization are given in [23]. Numerical details

that are pertinent to the TDSE solution can be found in [25–27].

The TDSE (2) is driven by the electric field $E(t)$ composed of co-linearly \hat{z} -polarized XUV and IR fields. The XUV field is represented by an APT

$$E_{\text{APT}}(t) = \sum_{\nu=-\lfloor N_{\text{APT}}/2 \rfloor}^{\lfloor N_{\text{APT}}/2 \rfloor} (-1)^\nu f_{\text{env}}(t_\nu) E_{\text{XUV}}(t-t_\nu), \quad (4)$$

where $N_{\text{APT}} = 41$ and the arrival time of each pulse $t_\nu = \nu T_{\text{IR}}/2$ is a half integer of the period of the IR oscillation $T_{\text{IR}} = 2\pi/\omega$. The envelope of the APT is modeled as

$$f_{\text{env}}(t) = \exp[-2 \ln 2(t/\tau_{\text{APT}})^2], \quad (5)$$

where τ_{APT} is the full width at half maximum (FWHM) of the train. Each ultrashort XUV pulse in the train takes the form

$$E_{\text{XUV}}(t) = E_{\text{XUV}} \exp[-2 \ln 2(t/\tau_{\text{XUV}})^2] \cos \Omega t, \quad (6)$$

with τ_{XUV} being the FWHM of the pulse. The XUV central frequency Ω and the time constants $\tau_{\text{XUV}}, \tau_{\text{APT}}$ are chosen to span a sufficient number of harmonics in the range of photon frequencies of interest for a given target. The IR pulse has a \cos^4 envelope and is shifted from the center of the APT by a variable delay τ . The XUV and IR intensities are 1×10^{14} W/cm² and 1×10^{10} W/cm², respectively. As both the XUV and IR fields are weak, we can calculate contributions of each XUV pulse to ionization, and after that summarize this contributions to get ionization amplitude for all the train [19]. Due to such a split, we can assume evolution in the field of just a single XUV pulse dressed by the IR field

$$E_\nu(t) = E_{\text{XUV}}(t) + E_{\text{IR}}(t - \tau - t_\nu). \quad (7)$$

The resulting ionization amplitude $A_{n\nu}(\mathbf{k})$ in such a field becomes a function of the photoelectron momentum \mathbf{k} and the quantum number n characterizing the residual ion. It can be used to construct the two-photon XUV+IR ionization amplitude in the XUV+IR field by performing the summation [19]

$$A_n(\mathbf{k}) = \sum_{\nu=-\lfloor N_{\text{APT}}/2 \rfloor}^{\lfloor N_{\text{APT}}/2 \rfloor} (-1)^\nu f_{\text{env}}(t_\nu) e^{i(\epsilon_n + k^2/2 - E_0)t_\nu} A_{n\nu}(\mathbf{k}), \quad (8)$$

where E_0 is the ground state energy. If the IR pulse is so long that the change in its envelope over time τ_{APT} is negligible, it is sufficient to calculate $A_{n0}(\mathbf{k})$ and $A_{n1}(\mathbf{k})$ only, because in this case $A_{n\nu}(\mathbf{k}) \simeq A_{n,|\nu| \bmod 2}(\mathbf{k})$. The pure two-photon ionization amplitude can be expressed as the difference $A_{n \text{ 2photon}}(\mathbf{k}) = A_{n0}(\mathbf{k}) - A_{n \text{ XUV}}(\mathbf{k})$.

If the system under consideration is an atom or a symmetric molecule, the number of required calculations is further reduced, as in this case, $A_{n1}(\mathbf{k}) = P_n A_{n0}(-\mathbf{k})$, where P_n is the parity of the n 's ionic state.

The pure two-photon ionization amplitude can be extracted by a simple symmetrization $A_n(\mathbf{k}) = [A_{n0}(\mathbf{k}) + P_n A_{n0}(-\mathbf{k})]/2$.

When solving the TDSE (2), the radial dependence of the wave function is handled by the discrete variable representation (DVR) on the finite elements of the Gauss-Lobatto quadrature. The angular dependence was represented by a spherical harmonic expansion [25]. The time evolution in Eq. (2) was carried out using an implicit fourth-order scheme [26], which is a generalization of the Crank-Nicholson scheme. The system of linear equations to which this scheme leads was solved using the biconjugate gradient method with a preconditioner. Suppression of the unphysical reflection from the radial grid boundary was carried out using exterior complex scaling (ECS) for the radial variable. Ionization amplitudes were extracted from the calculated wave function using the t-SURFFc method [27].

III. RESULTS

A. Autoionizing states

The continuously resolved spectrum of the AIS in He is displayed in Fig. 1. The AIS energies and identification are marked on the top horizontal axis according to [28]. The top (red) spectrum corresponds to XUV ionization only. Such a spectrum can be compared directly with the synchrotron measurement [28]. Each resonant state can be characterized by the corresponding set of the Fano parameters which are listed in Table I. The bottom (green) spectrum corresponds to XUV+IR ionization. The corresponding AIS can be derived from the red spectrum by absorption or emission of a single IR photon $\pm\omega$ indicated by arrows in Fig. 1. The parameters of these two-photon states, also tabulated, have no analogue in synchrotron measurements. Moreover, these states decay to the two non-resonant continua. Hence their Fano parameterization differ qualitatively with the need of introducing a correlation factor ρ^2 [29]

$$\sigma(E) = \sigma_0 \left[1 - \rho^2 + \rho^2 \frac{(q + \epsilon)^2}{1 + \epsilon^2} \right], \quad \epsilon = \frac{E - E_0}{\Gamma/2}. \quad (9)$$

Such an index $\rho^2 = 1$ in the XUV only spectrum of He.

As is seen in the table, the conventional Fano parameters of the $ns2+$ and $ns3+$ states are very close between the present theoretical determination and the experiment [28]. Generally, the TDSE should be propagated for the times exceeding the corresponding lifetime and this would become unpractical for very long-living higher members of the $spn+$ series, not shown in the table. The resonances in the XUV+IR spectrum are noticeably broader as their seeming lifetime is determined by an overlap with the IR probe pulse. Outside this overlap, the AIS does not contribute to the two-photon ionization amplitude [24].

As was shown in [21], the knowledge of the Fano parameters permits to derive the resonant phase and the

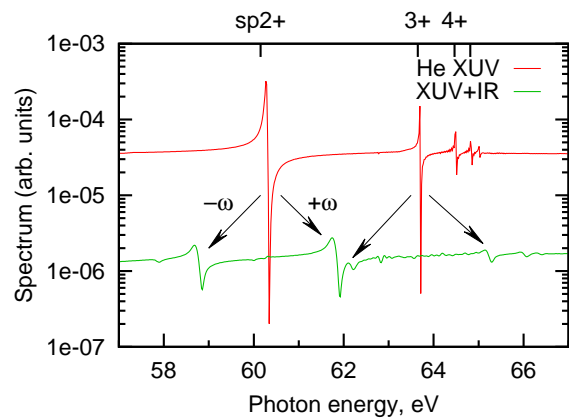


FIG. 1: Photoelectron spectra of He in single XUV photon (top, red) and XUV+IR (bottom, green) ionization. The corresponding AIS are marked on the top horizontal axis according to [28]. The arrows indicate the genesis of the resonant peaks in the XUV+IR spectrum. The laser photon energy $\omega = 1.53$ eV

corresponding atomic time delay. The amplitude-phase transformation is based on the Kramers-Kronig relation expressed via a logarithmic Hilbert transform (LHT). Validity of this transformation was demonstrated in [21] in several cases of resonant photoionization induced by a single XUV photon absorption. Here we apply the same technique to relate the RABBITT amplitude B and phase C parameters. More specifically, we convert the XUV+IR Fano parameters from Table I into an alternative set $r = \rho^{-2} - 1$, $Q = q/(r + 1)$ and $\gamma = \sqrt{r(r + q^2 + 1)}/(r + 1)^2$ to express the phase as pre-

TABLE I: Fano parameters of the AIS in He and H_2 . The present theoretical values extracted from the XUV-only spectra are compared with the He measurement [28] and an earlier H_2 calculation [30]. In the latter case, the two lowest AIS of the $^1\Sigma_u$ symmetry are shown.

	XUV only		XUV+IR			
	$2sp+$	$3sp+$	$2sp+$	$2sp+$	$-\omega$	$+\omega$
	TDSE	Ref.	TDSE	Ref.		
He atom		[28]		[28]		
q	-2.95	-2.75	-2.46	-2.5	-0.93	-1.03
Γ , meV	43	37	8	10	126	137
E_0 , eV	60.28	60.15	63.70	63.65	58.7	61.8
ρ^2					0.53	0.59
H_2 molecule		[30]		[30]		
q	-0.75		-0.86		-0.47	
Γ , meV	400	430	137	100	367	
E_0 , eV	30.3	30.1	32.3	32.3	29.1	
ρ^2					0.73	

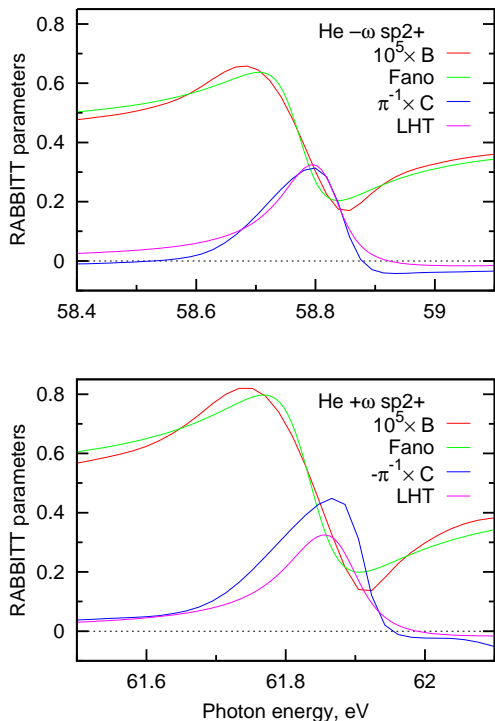


FIG. 2: Resonant B and C parameters are displayed with the corresponding Fano ansatz (9) and the LHT transform (11) for the $\pm\omega$ shifted $sp2+$ resonance in He.

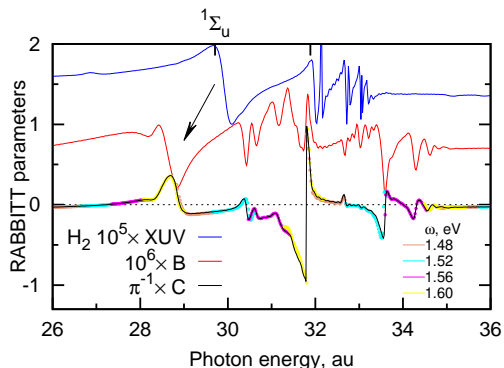


FIG. 3: Resonant B and C parameters in XUV+IR ionization of the H_2 molecule at the equilibrium internuclear distance of $R = 1.4$ au. The XUV-only spectrum, also shown, is shifted upwards for clarity. The two lowest AIS of the $1\Sigma_u$ symmetry are marked on the top horizontal axis according to [30]. The C parameters extracted from r RABBITT calculations at fixed photon energies are marked by rainbow colors. Four r RABBITT calculations are needed instead of a single cr RABBITT one.

scribed by of Eq. (19) of [21]

$$C = \arg [1 + [Q + i(\gamma - 1)](\epsilon + i)^{-1}] \quad (10)$$

Both the Fano fit for the B parameter and the LHT result for the C parameter are displayed in Fig. 2 for the $\pm\omega$ shifted $2sp+$ resonance. This figure demonstrates that

the amplitude-phase relation is generally valid in the case of two-photon XUV+IR ionization when the resonance is embedded in only one of the two RABBITT arms. This relation would be difficult to establish if two or more resonances are intertwined in the neighboring absorption and emission channels.

The resonant XUV+IR spectrum of the H_2 molecule at the equilibrium internuclear distance $R = 1.4$ au is displayed in Fig. 3. As compared to the corresponding spectrum of the He atom exhibited as the green line in Fig. 1 and in more detail in Fig. 2, the H_2 molecule demonstrates a considerably richer spectrum of several partially overlapping resonant states. The two lowest states of the $1\Sigma_u$ symmetry can be resolved sufficiently accurately from the XUV-only spectrum with the Fano parameters listed in Table I. These parameters compare favorably with the literature values [30].

B. Below threshold excitations

Finally, we apply our cr RABBITT technique to look under the threshold and to resolve a series of single-electron $1s \rightarrow np$ excitations in He. Here we utilize the u RABBITT methodology which is based on the following consideration (see e.g. [22]). When the laser photon energy is such that $(2q - 1)\omega < I_p < 2q\omega$, the harmonic peak H_{2q-1} submerges below the ionization threshold while the adjacent SB_{2q} is still visible in the photoelectron spectrum. As ω varies, H_{2q-1} crosses a number of discrete below-threshold excitations and the magnitude and phase parameters of SB_{2q} change rapidly. The cr RABBITT technique allows to look inside this near-threshold SB_{2q} without the need for adjusting ω . Moreover, our determination allows to span the whole series of the below-threshold discrete excitations in a single TDSE run.

This is illustrated in Fig. 4 where we display the B and C parameters in He in the near-threshold region. For the clarity of presentation, we choose a rather high central photon energy of $\omega = 6.1$ eV such that the corresponding photoelectron spectrum is stretched sufficiently far away from the threshold. As the photoelectron energy varies, the corresponding position of the submerged harmonic H_3 intersects with the series of discrete excitations $1s \rightarrow np$ whose energies, shifted upwards by ω , are marked on the top horizontal axis of the plot. Each of such crossing is accompanied by a sharp peak of the magnitude B parameter. These peaks are broadened with the spectral width of the APT. At the same time, the phase C parameter undergoes a series of π jumps dampened by a finite spectral width. This jumps can be reproduced closely by a numerical LHT

$$C(E) = -\frac{1}{\pi} \mathcal{P} \int_0^{E_{\max}} dx \frac{\ln B(x)}{x - E} \approx -\frac{1}{\pi} \mathcal{P} \int_{-\infty}^{\infty} dx \frac{\ln B(x)}{x - E}. \quad (11)$$

Eq. (11) represents the Kramers-Kronig relation connect-

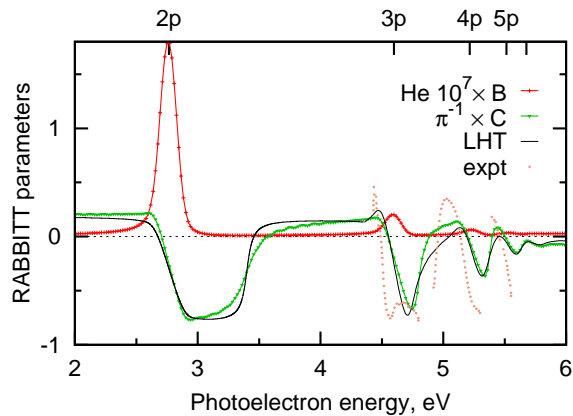


FIG. 4: RABBITT magnitude B and phase C parameters in He near threshold shown as functions of the photoelectron energy. The data points represent the measured phase [6]. The thin solid line visualizes the LHT (11).

ing the imaginary and real parts of the logarithm of a complex function. In this equation, the principal value integral, taken across the photoelectron spectrum, is extended to infinite limits where the resonant spectrum is vanishing. The integration in Eq. (11) is performed using the numerical recipe [31]. Correction is also needed for the vanishing amplitude $f(E)$ which makes the logarithmic derivative $f'(E)/f(E)$ divergent [32, 33] Such LHT calculated C parameter is sufficiently close to the TDSE calculation. Both are qualitatively similar to the experimental values [6].

IV. CONCLUSION

In conclusion, we realize the continuous rainbow cr RABBITT based on the parity separation of the XUV+IR ionization amplitude. Our procedure allows to achieve a very fine energy resolution across a wide spectrum without the need for adjusting the laser photon frequency. We demonstrate a great computational efficiency of the cr RABBITT technique in which the magnitude and phase parameters of the resonant states can be extracted for the whole series of resonances, both below and above the ionization threshold. This is a considerable improvement in comparison with the need for the laser frequency adjustment in r RABBITT that is required to span several resonant peaks in the photoelectron spectrum.

We apply the cr RABBITT to resolve the series of AIS in the He atom and the H_2 molecule. In addition, we look under the threshold in the spirit of the u RABBITT investigation and resolve the whole series of the $1s \rightarrow np$ discrete excitations in the He atom. We also apply the logarithmic Hilbert transform to utilize the Kramers-Kronig relation and to link the magnitude and phase RABBITT parameters in the resonant ionization of the He atom. This is the first successful application of the LHT to two-photon ionization processes.

While the present work demonstrates an application of cr RABBITT to two-electron targets such as He and H_2 , more complicated atomic and molecular systems can be treated in a similar way. This would only require an expansion of the multi-configuration basis (3) built from a greater number of one-electron orbitals. Only one such orbital needs to be continuous while others could be built from the discrete ionic states.

Finally, while the parity-based amplitude separation is not feasible experimentally, the XUV+IR and XUV-only components of the photoelectron wavepacket can be separated based on their distinct angular distributions.

In the future development, we intend to apply the cr RABBITT technique to the RABBITT process driven by circularly polarized radiation. Such a circularly polarized RABBITT allows to retrieve the amplitude ratios and phase difference in the two ionization channels accessible by the XUV+IR absorption [34, 35]. The under-threshold behavior of the circular RABBITT has never been investigated before and the present cr RABBITT technique will be highly computationally efficient for this purpose.

Acknowledgment:

We thank Rowan Jesson Kerr for his help with numerical implementation of the LHT. This work was supported by the Discovery Grant DP230101253 from the Australian Research Council.

- [1] K. Klünder, J. M. Dahlström, M. Gisselbrecht, T. Fordell, M. Swoboda, D. Guénot, P. Johnsson, J. Caillat, J. Mauritsson, A. Maquet, et al., *Probing single-photon ionization on the attosecond time scale*, Phys. Rev. Lett. **106**, 143002 (2011).
- [2] M. Kotur, D. Guénot, Jiménez-Galán, D. Kroon, E. W. Larsen, M. Louisy, S. Bengtsson, M. Miranda, J. Mauritsson, C. L. Arnold, et al., *Spectral phase measurement of a Fano resonance using tunable attosecond pulses*, Nature Communications **7**, 10566 (2016).
- [3] V. Gruson, L. Barreau, Á. Jiménez-Galan, F. Risoud, J. Caillat, A. Maquet, B. Carré, F. Lepetit, J.-F. Hergott, T. Ruchon, et al., *Attosecond dynamics through a Fano resonance: Monitoring the birth of a photoelectron*, Science **354**(6313), 734 (2016).
- [4] D. Busto, L. Barreau, M. Isinger, M. Turconi, C. Alexandridi, A. Harth, S. Zhong, R. J. Squibb, D. Kroon, S. Plogmaker, et al., *Time-frequency representation of autoionization dynamics in helium*, J. Phys. B **51**(4), 044002 (2018).
- [5] M. Isinger, D. Busto, S. Mikaelsson, S. Zhong, C. Guo, P. Salières, C. L. Arnold, A. L’Huillier, and M. Gisselbrecht, *Accuracy and precision of the rabbit technique*, Phil. Trans. Royal Soc. A **377**(2145), 20170475 (2019).
- [6] L. Neoricic, D. Busto, H. Laurell, R. Weissenbilder, M. Ammitzböll, S. Luo, J. Peschel, H. Wikmark, J. Lahl, S. Maclot, et al., *Resonant two-photon ionization of helium atoms studied by attosecond interferometry*, Frontiers in Physics **10** (2022).
- [7] M. Turconi, L. Barreau, D. Busto, M. Isinger, C. Alexandridi, A. Harth, R. J. Squibb, D. Kroon, C. L. Arnold, R. Feifel, et al., *Spin-orbit-resolved spectral phase measurements around a fano resonance*, J. Phys. B **53**(18), 184003 (2020).
- [8] L. Roantree, J. Wragg, H. van der Hart, and A. Brown, *Energy- and angle-resolved spectral phases via semirelativistic ab initio rabbit simulations*, Phys. Rev. A **108**, 023112 (2023).
- [9] C. Alexandridi, D. Platzter, L. Barreau, D. Busto, S. Zhong, M. Turconi, L. Neoricic, H. Laurell, C. L. Arnold, A. Borot, et al., *Attosecond photoionization dynamics in the vicinity of the Cooper minima in argon*, Phys. Rev. Research **3**, L012012 (2021).
- [10] V. J. Borràs, J. González-Vázquez, L. Argenti, and F. Martín, *Attosecond photoionization delays in the vicinity of molecular Feshbach resonances*, Science Advances **9**(15), eade3855 (2023).
- [11] M. Swoboda, T. Fordell, K. Klünder, J. M. Dahlström, M. Miranda, C. Buth, K. J. Schafer, J. Mauritsson, A. L’Huillier, and M. Gisselbrecht, *Phase measurement of resonant two-photon ionization in helium*, Phys. Rev. Lett. **104**, 103003 (2010).
- [12] L. Barreau, C. L. M. Petersson, M. Klinker, A. Camper, C. Marante, T. Gorman, D. Kiesewetter, L. Argenti, P. Agostini, J. González-Vázquez, et al., *Disentangling spectral phases of interfering autoionizing states from attosecond interferometric measurements*, Phys. Rev. Lett. **122**, 253203 (2019).
- [13] L. Drescher, T. Witting, O. Kornilov, and M. J. J. Vrakking, *Phase dependence of resonant and antiresonant two-photon excitations*, Phys. Rev. A **105**, L011101 (2022).
- [14] D. M. Villeneuve, P. Hockett, M. J. J. Vrakking, and H. Niikura, *Coherent imaging of an attosecond electron wave packet*, Science **356**(6343), 1150 (2017).
- [15] A. S. Kheifets and A. W. Bray, *RABBITT phase transition across the ionization threshold*, Phys. Rev. A **103**, L011101 (2021).
- [16] A. Kheifets, *Revealing the target electronic structure with under-threshold RABBITT*, Atoms **9**(3), 66 (2021).
- [17] A. S. Kheifets, *Under-threshold RABBITT in argon*, J. Phys. B **56**(9), 095201 (2023).
- [18] M. Moiola, M. Popova, K. Hamilton, D. Ertel, D. Busto, I. Makos, M. Kiselev, S. Yudin, H. Ahmadi, C. Schröter, et al., *Role of intermediate resonances in attosecond photoelectron interferometry in neon*, arXiv preprint arXiv:2410.04240 (2024).
- [19] V. V. Serov and A. S. Kheifets, *Angular anisotropy of time delay in XUV+IR photoionization of H_2^+* , Phys. Rev. A **93**, 063417 (2016).
- [20] V. V. Serov and A. S. Kheifets, *Time delay in XUV/IR photoionization of H_2O* , J. Chem. Phys. **147**(20), 204303 (2017).
- [21] J.-B. Ji, A. S. Kheifets, M. Han, K. Ueda, and H. J. Wörner, *Relation between photoionisation cross sections and attosecond time delays*, New J. Phys. **26**(9), 093014 (2024).
- [22] A. S. Kheifets, *Resonant photoionization and time delay*, arXiv preprint arXiv:2410.16696 (2024).
- [23] V. Serov, *Time-dependent convergent close coupling method for molecular ionization in laser fields*, arXiv preprint arXiv:2405.12455 (2024).
- [24] V. V. Serov and A. S. Kheifets, *Fano-line-shape metamorphosis in resonant two-photon ionization*, Physical Review A **110**(4), 043107 (2024).
- [25] V. V. Serov, *Calculation of intermediate-energy electron-impact ionization of molecular hydrogen and nitrogen using the paraxial approximation*, Phys. Rev. A **84**, 062701 (2011).
- [26] I. Puzynin, A. Selin, and S. Vinitzky, *Magnus-factorized method for numerical solving the time-dependent Schrödinger equation*, Comp. Phys. Comm. **126**(1), 158 (2000).
- [27] V. V. Serov, V. L. Derbov, T. A. Sergeeva, and S. I. Vinitzky, *Hybrid surface-flux method for extraction of the ionization amplitude from the calculated wave function*, Phys. Rev. A **88**, 043403 (2013).
- [28] M. Domke, K. Schulz, G. Remmers, G. Kaindl, and D. Wintgen, *High-resolution study of $^1P^o$ double-excitation states in helium*, Phys. Rev. A **53**, 1424 (1996).
- [29] U. Fano and J. W. Cooper, *Line profiles in the far-uv absorption spectra of the rare gases*, Phys. Rev. **137**, A1364 (1965).
- [30] I. Sánchez and F. Martín, *The doubly excited states of the H_2 molecule*, J. Chem. Phys. **106**(18), 7720 (1997).
- [31] P. Virtanen, R. Gommers, T. E. Oliphant, M. Haberland, T. Reddy, D. Cournapeau, E. Burovski, P. Peterson, W. Weckesser, J. Bright, et al., *SciPy 1.0: Fundamental Algorithms for Scientific Computing in Python*, Nature Methods **17**, 261 (2020).

- [32] R. E. Burge, M. A. Fiddy, A. H. Greenaway, and G. Ross, *The application of dispersion relations (Hilbert transforms) to phase retrieval*, J. Phys. D **7**(6), L65 (1974).
- [33] R. E. Burge, M. A. Fiddy, A. H. Greenaway, G. Ross, and W. C. Price, *The phase problem*, Proc. Royal Soc. London. A **350**(1661), 191 (1976).
- [34] A. S. Kheifets, *Characterization of XUV+IR ionization using the circular dichroic phase*, Phys. Rev. Res. **6**(1), L012002 (2024).
- [35] A. S. Kheifets, *Circularly polarized RABBITT on atomic shells with large orbital momentum*, J. Phys. B **58**(4), 045601 (2025).